AGU PUBLICATIONS

JGR

Journal of Geophysical Research: Space Physics

RESEARCH ARTICLE
10.1002/2017JA024211

Key Points:
- Statistical study of ELF/VLF emissions simultaneously observed at three ground-based stations
- Longitudinal extent of ELF/VLE emissions and the dependence of *AE* and *Dst* indices
- Dependence of wave occurrence rates on MLT at multiple stations

Correspondence to:
K. Shiokawa,
shiokawa@nagoya-u.jp

Citation:
Yonezu, Y., K. Shiokawa, M. Connors, M. Ozaki, J. Manninen, H. Yamagishi, and M. Okada (2017), Simultaneous observations of magnetospheric ELF/VLF emissions in Canada, Finland, and Antarctica, *J. Geophys. Res. Space Physics*, *122*, 6442–6454, doi:10.1002/2017JA024211.

Received 30 MAR 2017
Accepted 13 JUN 2017
Accepted article online 15 JUN 2017
Published online 28 JUN 2017

Simultaneous observations of magnetospheric ELF/VLF emissions in Canada, Finland, and Antarctica

Yusuke Yonezu[1], Kazuo Shiokawa[1], Martin Connors[2], Mitsunori Ozaki[3], Jyrki Manninen[4], Hisao Yamagishi[5], and Masaki Okada[5]

[1]Institute for Space-Earth Environmental Research, Nagoya University, Nagoya, Japan, [2]Centre for Science, Athabasca University, Athabasca, Alberta, Canada, [3]Faculty of Electrical and Computer Engineering, Institute of Science and Engineering, Kanazawa University, Kanazawa, Japan, [4]Sodankyla Geophysical Observatory, University of Oulu, Sodankyla, Finland, [5]National Institute of Polar Research, Tachikawa, Japan

Abstract To investigate longitudinal extent of electromagnetic wave activity, we report the first simultaneous ground-based observations of magnetospheric ELF/VLF emissions at the following three longitudinally separated stations at auroral and subauroral latitudes: Athabasca, Canada (ATH; magnetic latitude: 61.3°N); Kannuslehto, Finland (KAN; 64.4°N); and Syowa Station, Antarctica (SYO; 70.5°S). The magnetic local time (MLT) separations of SYO-KAN, ATH-SYO, and ATH-KAN, are 3, 8, and 11 h, respectively. Simultaneous observation data at these stations are available for a total of 48 days in 2012–2014. The simultaneous occurrence rates of ELF/VLF emissions are 9.8%, 2.5%, and 3.6% for SYO-KAN, ATH-SYO, and ATH-KAN, respectively. We found that the simultaneous wave occurrence rate between two stations is higher in the morning-dayside sector, indicating that the longitudinal extent of the emissions exhibits MLT dependence. When emissions are simultaneously observed at two stations, the average *AE* and |*Dst*| indices tend to be higher. Similarly, if the two stations are more separated in MLT, the average |*Dst*| index increases. These results suggest that the longitudinal extent of ELF/VLF emissions increases with increasing geomagnetic activity.

1. Introduction

Extremely low frequency (ELF) and very low frequency (VLF) chorus emissions are generated in the Earth's inner magnetosphere and propagate to the ground through density ducts along the geomagnetic field lines [e.g., *Helliwell*, 1965] or through nonducted propagation oblique to the geomagnetic field line [e.g., *Chum and Santolik*, 2005; *Golden et al.*, 2010]. ELF/VLF emissions generated in the inner magnetosphere mainly arise from electron temperature anisotropy on magnetic field lines near the equatorial plane [e.g., *Kennel and Petschek*, 1966; *Sazhin and Hayakawa*, 1992; *Omura et al.*, 2009; *Li et al.*, 2009a]. The major magnetospheric ELF/VLF emission types are chorus, hiss, and quasiperiodic (QP) [e.g., *Helliwell*, 1965]. Chorus emissions are a population of discrete elements of intense electromagnetic waves observed at high latitudes. Chorus emissions help accelerate electrons to relativistic energies in the radiation belts [e.g., *Meredith et al.*, 2003, *Miyoshi et al.*, 2003, 2015; *Horne et al.*, 2005]. Hiss emissions have a noise-like structure and are continuously observed over wide frequency ranges. Plasmaspheric hiss are caused as a result of propagation of ELF/VLF chorus waves [e.g., *Thorne et al.*, 1973; *Bortnik et al.*, 2008; *Chen et al.*, 2012a, 2012b], although the possibility of lightning generation of plasmaspheric hiss emissions is also discussed [e.g., *Dowden*, 1971; *Sonwalkar and Inan*, 1989; *Meredith et al.*, 2006]. In contrast, QP emissions have a clear structure that exhibits a quasiperiodic modulation of intensity and frequency with time. The period of the intensity modulation is from 10 s to a couple of minutes [e.g., *Carson et al.*, 1965; *Sato and Kokubun*, 1980; *Sato and Fukunishi*, 1981; *Smith et al.*, 1998]. These ELF/VLF individual emissions have been studied for several decades.

Previous simultaneous observation of ELF/VLF emissions with multipoint ground-based stations has been performed using geomagnetic conjugate points or relatively closely spaced station pairs. *Sato and Kokubun* [1980] investigated the interaction between ELF/VLF emissions and magnetic pulsations by using geomagnetic conjugated points comprising the Syowa and Mizuho stations in Antarctica and Husafell in Iceland. They found that each QP element is simultaneously observed at the conjugate point with an accuracy of 1 s. This symmetry indicates that the interaction between whistler mode waves and hydromagnetic waves occurs near

the equator in the magnetosphere. *Manninen et al.* [2014] and *Martinez-Calderon et al.* [2015a] reported VLF emissions simultaneously observed at two separated stations with a separation of about 400–450 km and identified the ionospheric exit area of the emissions through the polarization analysis of the waves.

Statistical studies of ELF/VLF emissions have also been performed by using ground-based and satellite instruments. The occurrence of ELF/VLF emissions as a function of magnetic local time (MLT) has been statistically investigated. In situ observations by using OGO 5 satellite [e.g., *Tsurutani and Smith*, 1977] have shown that chorus emissions are most intense and occur frequently in the postmidnight and dawn-to-noon hours at auroral L values. Statistical analyses using Time History of Events and Macroscale Interactions during Substorms (THEMIS) satellites have revealed the dependence of global distribution of chorus waves on geomagnetic activity, confinement of nightside emissions to low magnetic latitudes, and extension of dayside emissions to high latitudes [e.g., *Li et al.*, 2009b; *Golden et al.*, 2012b; *Bunch et al.*, 2012]. Observations in the equatorial plane showed that chorus emissions are frequently generated between 0300 and 1000 MLT in the region $4 < L < 7$ [*Meredith et al.*, 2003]. Plasmaspheric hiss generally occurs between 0600 and 2100 MLT in the region $2 < L < 4$ [*Meredith et al.*, 2004]. Global hiss distribution measured by the THEMIS satellites showed that the peak local time of hiss emissions moves to the noon and postnoon sectors in the recovery phase of the storm at $2 < L < 5$ [*Golden et al.*, 2012a; *Kim et al.*, 2015]. On the other hand, the high-amplitude region of chorus moves from the prenoon sector to the midnight sector during disturbed conditions [*Kim et al.*, 2013].

Ground-based observations of ELF/VLF emissions [e.g., *Pope*, 1960; *Spasojevic*, 2014] have also shown that the occurrence peak of chorus emissions is in the postmidnight and dawn-to-noon hours at auroral L values. Statistical studies of the latitudinal variation of ELF/VLF emissions have also been performed. *Smith et al.* [2010] reported on two ground-based observations at auroral latitudes that the morning chorus emission is at a later local time at higher-latitude stations. Recently, a study of ELF/VLF emissions at subauroal latitudes was performed by investigating the ELF/VLF wave data obtained at the Athabasca University Geophysical Observatory at $L = 4.3$ [*Martinez-Calderon et al.*, 2015b]. They investigated the occurrence rates of ELF/VLF emissions as a function of MLT, including chorus, hiss, and QP emissions, their seasonal variation, and the dependences of *AE* and *Dst* indices and geomagnetic and solar wind parameters. They found a maximum occurrence rate in the morning sector (0600 to 0700 MLT) and a minimum in the night sector (~1800 to 0200 MLT).

The relation between the generation of ELF/VLF emissions and substorms has also been studied [e.g., *Tsurutani and Smith*, 1977]. Equatorial chorus waves are generated primarily during substorms, whereas high-latitude chorus waves are not strongly dependent on the *AE* index [*Tsurutani and Smith*, 1977]. *Parrot and Gaye* [1994] reported that substorms ($AE > 300$ nT) increase the maximum average amplitudes of ELF emissions by a factor of 2.

As reviewed above, the temporal and spatial features of ELF/VLF emissions and their geomagnetic activity dependence have been investigated by several previous studies. However, the longitudinal extent of ELF/VLF emissions is not well understood because simultaneous multipoint ELF/VLF measurements separated in longitudes have not been available. In this paper, we investigate the longitudinal extent of ELF/VLF emissions by using simultaneous observations at three ground-based stations, which are longitudinally separated at subauroral and auroral latitudes. The advantage of ground-based observations is that we can monitor the ELF/VLF emissions at multiple fixed locations continuously.

2. Observation

2.1. Observatories and Method

We use ELF/VLF wave data obtained at three ground-based stations: Athabasca University Geophysical Observatory in Canada (ATH; 54.6°N, 246.4°E, magnetic latitude (MLAT) 61.3°N, L = 4.3); Kannuslehto in Finland (KAN; 67.7°, 26.3°, MLAT 64.4°, L = 5.3); and the Syowa Station in Antarctica (SYO; 69.0°S, 39.6°E, MLAT 70.5°S, L = 6.4). Figure 1 shows the coordinates of each station by magnetic latitude and MLT which are calculated by the International Geomagnetic Reference Field (IGRF) 10 model. There are 3, 8, and 11 h MLT differences between KAN-SYO, SYO-ATH, and KAN-ATH, respectively, in the dayside sector. Table 1 shows properties of the receivers to measure ELF/VLF waves. Delta-type loop antennas are used at Athabasca and Syowa Stations (details are available in *Ozaki et al.* [2008] and *Shiokawa et al.* [2014]), and two loop antennas are used at Kannuslehto [*Manninen*, 2005]. The sampling frequencies are 100 kHz for ATH, 78.125 kHz for KAN, and 4 (2012), 5 (2013), and 20 kHz (2014) for SYO. Both east-west and north-south magnetic field components of ELF/VLF waves were measured at ATH, KAN, and SYO in 2013 and 2014, whereas only one component

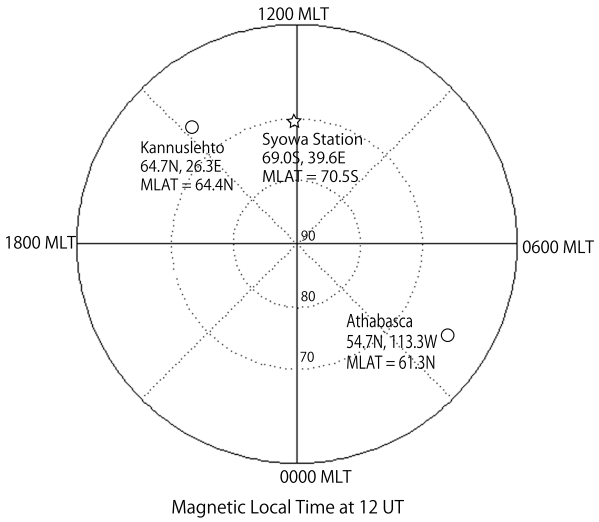

Figure 1. Coordinates of each station shown by magnetic latitude and MLT, which are calculated by the IGRF 10 model. The star and circles indicate stations located in the Southern and Northern Hemispheres, respectively. There are 3, 8, and 11 h MLT differences at KAN-SYO, SYO-ATH, and KAN-ATH, respectively, in the dayside sector.

(north-south) was obtained at SYO in 2012. The timing of data sampling is corrected by GPS receivers at these three stations. The data are stored as follows: 9 min 50 s of data recorded every 10 min at ATH; 60 min of data recorded every 60 min at KAN; and 1 min of data recorded every 1 min in 2012 and 2013 and 10 s of data record every 1 min in 2014 at SYO.

From the raw horizontal magnetic field data obtained by the loop antennas at ATH, we calculate the power spectral density (PSD) of ELF/VLF waves and obtain the dynamic spectra by fast Fourier transform (FFT) with 16,384 data points (0.16384 s). We average every 16 frequency data points to reduce FFT noise, obtaining the PSD with a frequency resolution of 97 Hz. We also consider the frequency dependence of the antenna sensitivity by applying calibration factors to convert the data unit from V^2/Hz to nT^2/Hz [e.g., *Martinez-Calderon et al.*, 2015a].

For KAN, we use a 16,384 point FFT to obtain dynamic spectra with a frequency resolution of 5 Hz. Similar calibration processing is also performed for the KAN spectra. For data analysis, special filters are used to reduce sferics and power line harmonic radiation. This technique is explained in *Manninen et al.* [2016]. The remaining fixed-frequency noises, which appear occasionally in the dynamic spectra, are due to the Russian ZEVS transmitter, which is located in Kola Peninsula at (68.8°N, 33.8°E) and at (68.7°N, 33.7°E), ~330 km northeast of KAN.

For SYO, we use a 512 point FFT to obtain 1 min spectra, with frequency resolutions of 125 Hz in 2012 and 156 Hz in 2013 and 2014. Calibration processing similar to that of ATH is also performed for the SYO spectra.

2.2. Data Definition

We examine the ELF/VLF wave spectra for 48 days for which the three stations (ATH, KAN, and SYO) have simultaneous measurements. Two plot types with time ranges of 10 min and 1 h are used for visual inspection of the ELF/VLF spectra. By inspecting 10 min plots, we first remove spectral data that contains intense lightning noise (sferics) to reduce the uncertainty of the distinction. We consider the following criteria to detect the magnetospheric ELF/VLF waves used in our analysis.

1. Clear ELF/VLF emissions that are not obscured by artificial noise or strong lightning activity and are clearly distinguishable from the background level by visual inspection.
2. Emission characteristics are clearly visible (e.g., discrete elements, QP features, and hiss continuous emissions) with frequency bands higher than 0.2 kHz.
3. The wave intensity is higher than $\sim 2 \times 10^{-11}$, $\sim 2 \times 10^{-13}$, and $\sim 2 \times 10^{-12}$ (nT^2/Hz) for ATH, KAN, and SYO, respectively. These values are the minimum values that we can distinguish from the background level by visual inspection.
4. Background noises at 1.5–4.0 kHz, 0.5–2.5 kHz, and 0.5–1.5 kHz for ATH, KAN, and SYO, are at least 1 order of magnitude smaller than the intensity of the observed ELF/VLF waves and does not cover more than 50%

Table 1. Receiver Properties

	Sampling Frequency	Antenna Type	Frequency Resolution	File Length
Athabasca	100 kHz	Delta	97 Hz	9 min 50 s
Kannuslehto	78.125 kHz	Square	5 Hz	60 min
Syowa Station	4 kHz (2012), 5 kHz (2013)	Delta	125 Hz (2012), 156 Hz (2013)	1 min

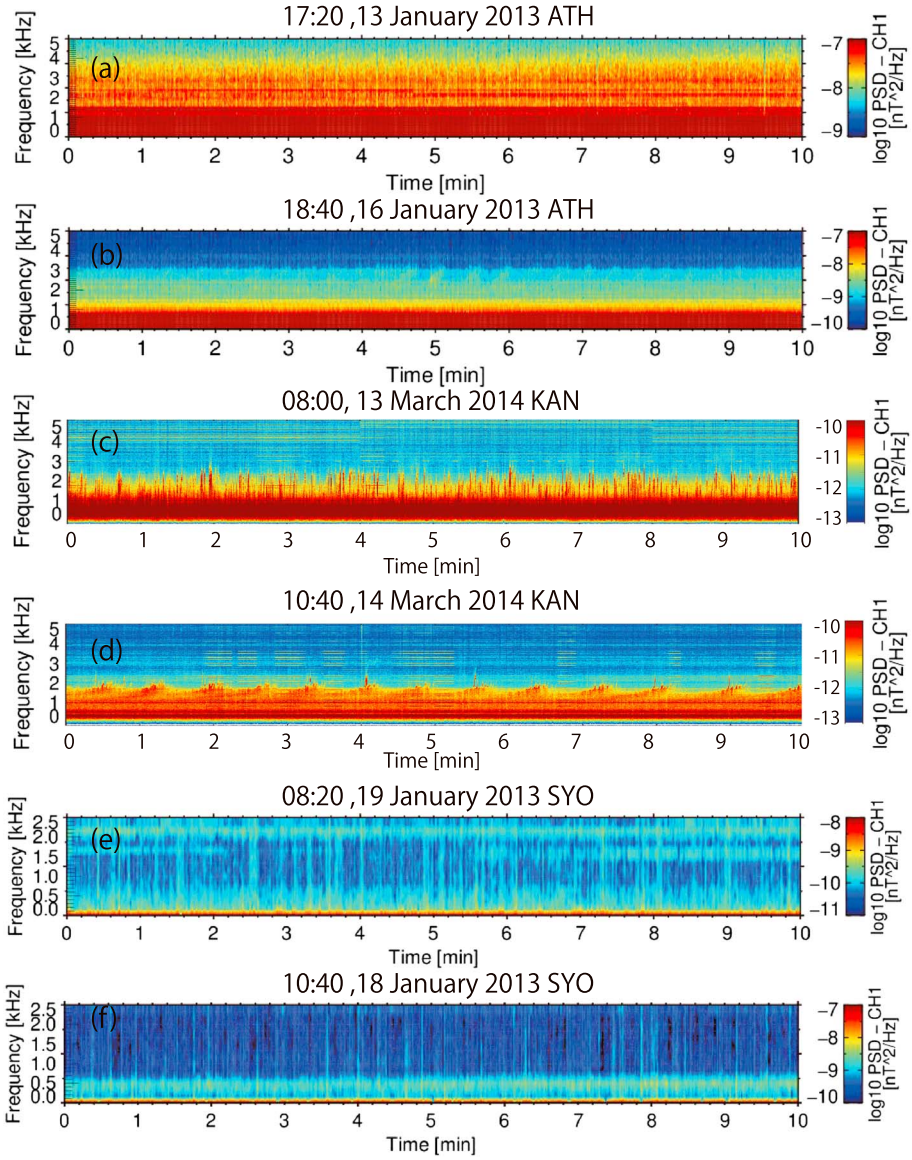

Figure 2. Examples of ELF/VLF emissions at (a, b) ATH, (c, d) KAN, and (e, f) SYO. Frequency ranges of the power spectrum are 0–5 kHz at ATH and KAN, and 0–2.5 kHz at SYO. Time ranges are 10 min at three stations. Color scales are from $\sim 1.0 \times 10^{-7}$ nT^2/Hz to $\sim 1.0 \times 10^{-9}$ nT^2/Hz for Figure 2a, from $\sim 1.0 \times 10^{-7}$ nT^2/Hz to $\sim 1.0 \times 10^{-10}$ nT^2/Hz for Figures 2b and 2f, from $\sim 1.0 \times 10^{-10}$ nT^2/Hz to $\sim 1.0 \times 10^{-13}$ nT^2/Hz for Figures 2c and 2d, and $\sim 1.0 \times 10^{-8}$ nT^2/Hz to $\sim 1.0 \times 10^{-11}$ nT^2/Hz for Figure 2e. Chorus/hiss emissions and QP emissions are shown in Figures 2a and 2c and Figures 2b and 2d, respectively, for ATH and KAN, whereas chorus and hiss emissions are shown in Figures 2e and 2f, respectively, for SYO.

of the spectra at this frequency range. These frequency ranges are chosen because of artificial noises at lower frequencies and lightning contamination at higher frequencies.

For the ATH spectra, we define the above criteria based on those of *Martinez-Calderon et al.* [2015b] to allow comparison with previous analysis. The wave frequency tends to decrease from ATH, KAN, to SYO, because the latitude increases from ATH, KAN, to SYO. For SYO data, additional criterion was applied that the spectral data exist for at least 5 min of a 10 min bin, because the raw data for SYO is stored every 1 min.

Figure 2 shows representative wave spectra at three stations. Chorus/hiss emissions are seen in Figures 2a and 2c for ATH and KAN, respectively, while the QP emissions are seen in Figures 2b and 2d. On the other hand, only chorus and hiss emissions are shown for SYO in Figures 2e and 2f, because there are no QP emissions at SYO for the analyzed period. The frequency ranges are 0–5 kHz for Figures 2a–2d and 0–2.5 kHz for

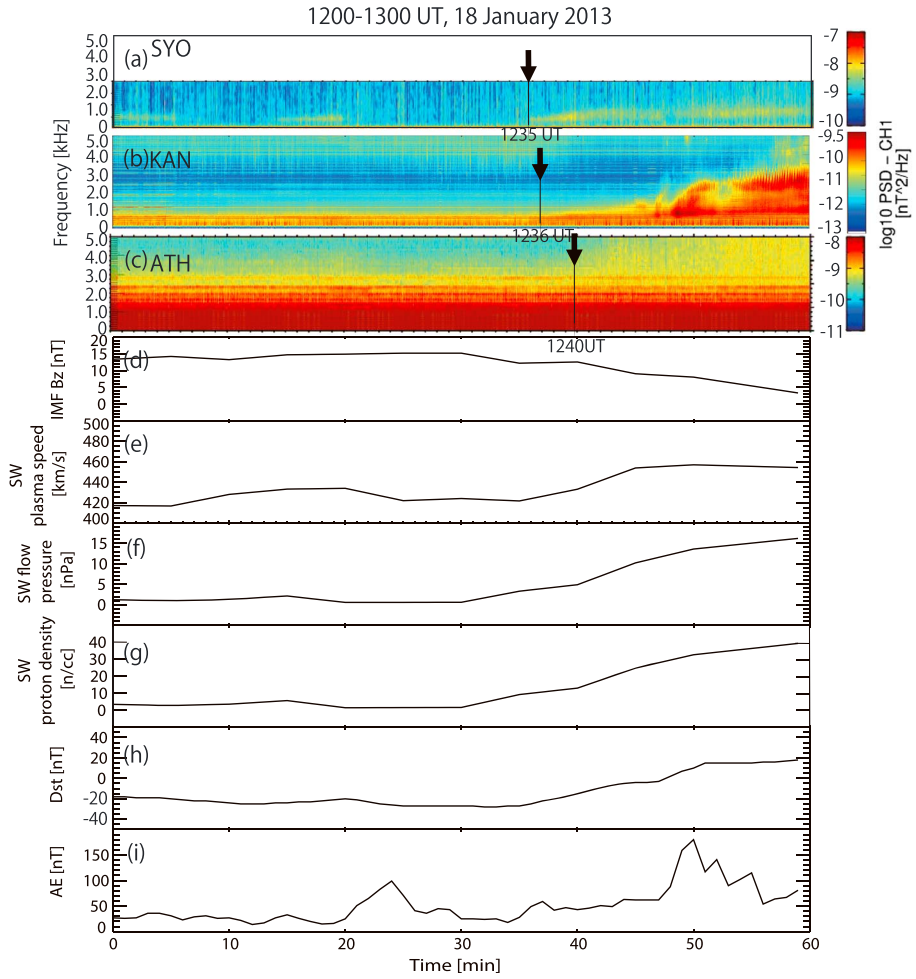

Figure 3. Event where hiss emissions are simultaneously observed at three stations at 1200–1300 UT on 18 January 2013, associated with an enhancement of solar wind dynamic pressure. Wave spectra at (a) SYO, (b) KAN, and (c) ATH. The vertical black lines with arrows show the onset of the hiss emissions. (d) IMF B_z component, (e) solar wind speed, (f) solar wind dynamic pressure, (g) solar wind proton density, and (h) *Dst* and (i) *AE* indices.

Figures 2e and 2f, and the color scales in Figure 2 also have differences of 3 orders in maximum. Based on these spectra, we categorized the ELF/VLF emissions as chorus/hiss or QP emissions. We regarded chorus and hiss emissions as one group. This is because the time and frequency resolution of the spectra obtained at SYO was too low to distinguish chorus and hiss. At ATH, bursty patches [e.g., *Shiokawa et al.*, 2014] are also observed for a total interval of about 10 h. We categorized these minor populations of bursty patches as chorus/hiss, because their spectral feature is basically that of chorus with short durations and they do not have repeating structures.

Figure 3 shows an event where hiss emissions are simultaneously observed at three stations at 12–13 UT on 18 January 2013. In this event, hiss emissions are observed sequentially at SYO, KAN, and ATH associated with a sudden enhancement of solar wind dynamic pressure. Figures 3a–3c illustrate the ELF/VLF wave spectra at frequencies of 0–2.5 kHz at SYO and 0–5.0 kHz at KAN and ATH, respectively. Figures 3d–3i show the interplanetary magnetic field (IMF) B_z component, speed, dynamic pressure, and proton density of solar wind, and *Dst* and *AE* indices, respectively. Figures 3a–3c and 3h indicate that the hiss emissions are observed at frequencies of 0.2–2.0 kHz at 1235 UT (1240 MLT) at SYO, from below 0.5 kHz to ~5 kHz at 1236 UT (1516 MLT) at KAN, and from ~2 kHz to above 5 kHz at 1240 UT (0440 MLT) at ATH, as indicated by the black arrows. This time interval is during the recovery phase of a weak geomagnetic storm, which has a maximum *Dst* index of −53 nT at 0000 UT on 18 January 2013. Figures 3e–3g indicate that the ELF/VLF emissions are observed at three stations associated with clear enhancement of solar wind dynamic pressure with increases of flow speed and plasma density. Figure 3d indicates that this event is not associated with the beginning of another storm

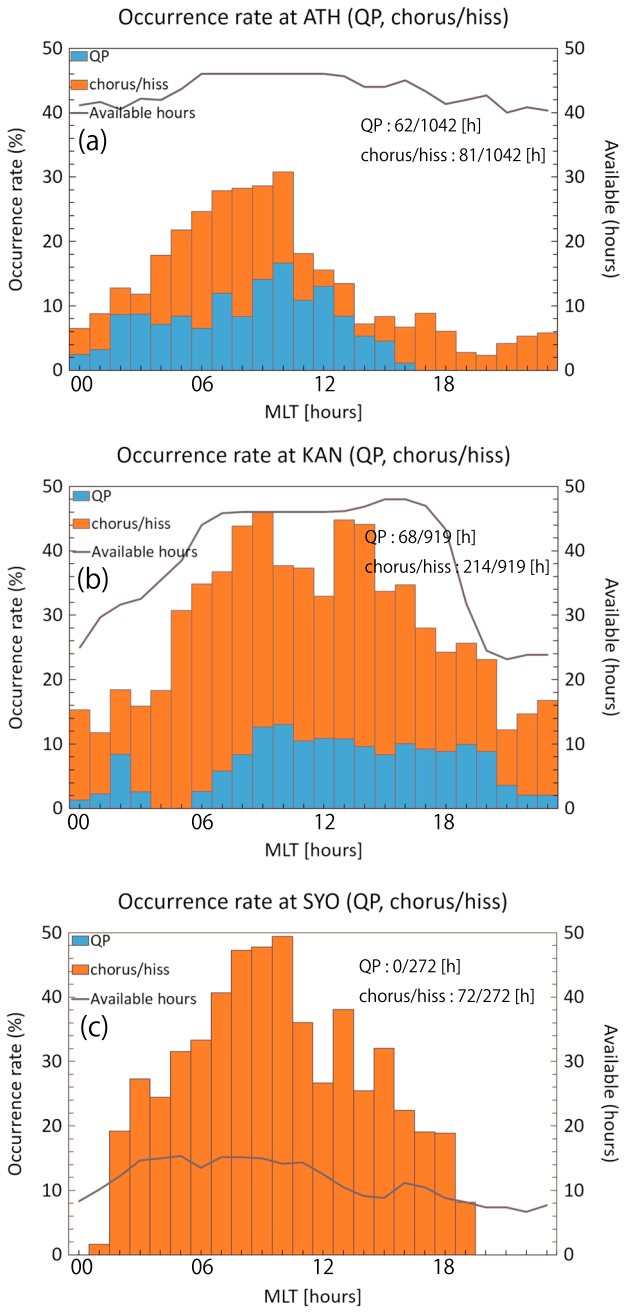

Figure 4. Occurrence rates of ELF/VLF emissions as a function of MLT at (a) ATH, (b) KAN, and (c) SYO. The black curve shows that actual available hours (data that contain intense lightning and shot noise is removed) per MLT for 48 days where the simultaneous data are available.

because the IMF remains northward. The *AE* index in Figure 3i increases twice, at 1220 and 1248 UT, with peaks of ~100 and ~180 nT, respectively, indicating that two small substorms took place at these times. However, it is unlikely that these substorms contributed to the generation of the ELF/VLF emissions observed at the three stations, because the start of the emission propagates from dayside (SYO and KAN) to nightside (ATH) and the second substorm started after the observed enhancement of ELF/VLF emissions. The observations in Figure 3 indicate that an enhancement of solar wind dynamic pressure can trigger magnetospheric ELF/VLF emissions on a global scale nearly simultaneously within 5 min, although simultaneous ELF/VLF emissions observed at three stations are rare, as shown below.

We statistically analyzed these magnetospheric ELF/VLF emissions as follows. First, to estimate the occurrence rate of the ELF/VLF waves at each station, we define 10 min bins for the 48 days analyzed at all stations. If we identify waves in a 10 min bin, we count it as one occurrence, even if more than two types of waves are observed during the 10 min. Then, we calculate the wave occurrence rates by dividing the number of bins with waves by the total available bins at each station.

In addition, we estimate the simultaneous occurrence rate of ELF/VLF emissions for two and three stations. We calculate time intervals (A) when the spectral data are simultaneously available for multiple stations, namely KAN-SYO, SYO-ATH, KAN-ATH, and KAN-SYO-ATH. Then, we count the number of 10 min bins (B) when waves are simultaneously observed at these pair stations. We calculate the simultaneous wave occurrence rate by dividing (B) by (A). Even if different types of waves are observed simultaneously at multiple stations, we count those as a simultaneous occurrence.

3. Results

3.1. Occurrence Rates at One Station

We estimate the occurrence rates of ELF/VLF emissions at ground-based stations by categorizing the emissions as chorus/hiss or QP emissions. Figures 4a–4c show total available hours (solid curves) and the occurrence rate (bars) of ELF/VLF waves, including QP and chorus/hiss emissions as a function of MLT at ATH, KAN, and SYO. The total number of available hours and the hours of QP and chorus/hiss emissions are shown on

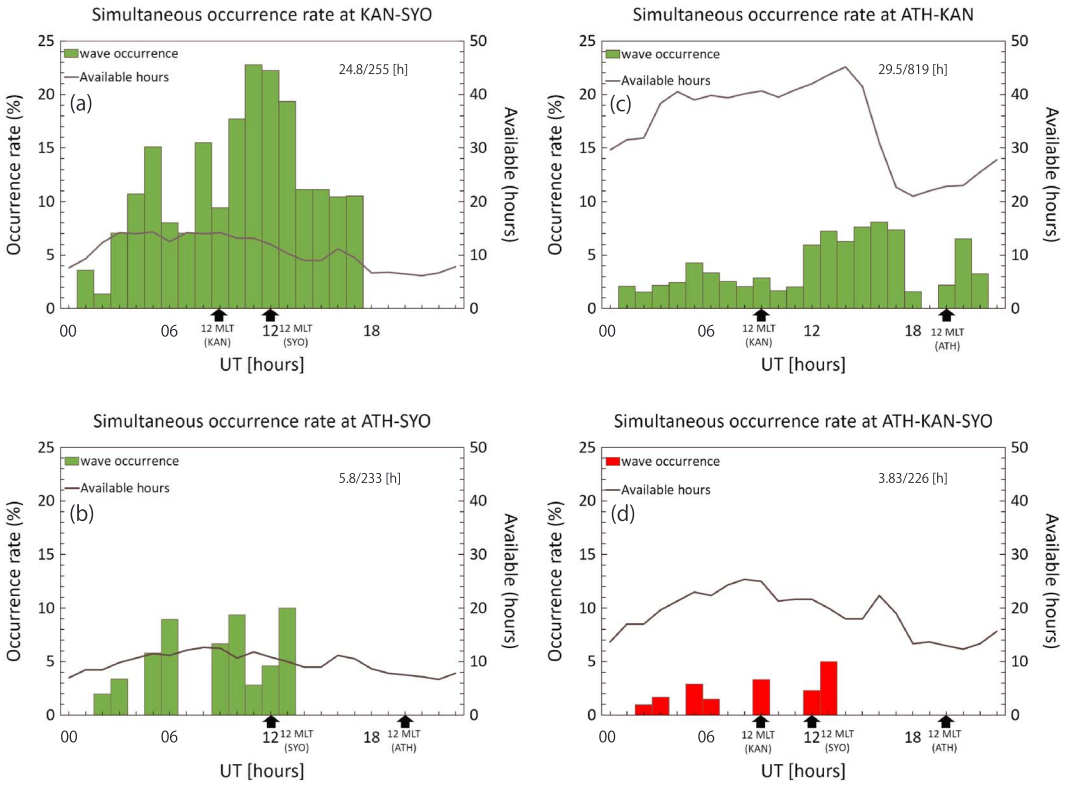

Figure 5. Simultaneous occurrence rate of ELF/VLF emissions for the (a) KAN-SYO, (b) ATH-SYO, (c) ATH-KAN, and (d) ATH-KAN-SYO data sets as a function of UT. The black curve shows the number of available hours per MLT hour.

the top right corner of each panel. All three stations have an occurrence peak in the morning at 1000 MLT at ATH, 0900 MLT at KAN, and 0800 to 1000 MLT at SYO, whereas there is another peak at 1300 MLT at auroral latitudes at SYO and KAN. The fractions of the QP emissions in all the ELF/VLF emissions is clearly higher at subauroral latitudes (43% (=62 h/(62 + 81) h)) at ATH) than at auroral latitudes (24% (=68 h/(68 + 214 h)) at KAN and 0% at SYO).

3.2. Simultaneous Occurrence Rates

Figure 5 shows the simultaneous occurrence rates of ELF/VLF emissions at two and three stations that are longitudinally/latitudinally separated as a function of UT. The total hours that waves are simultaneously observed and total available hours for each data set (ATH-KAN, KAN-SYO, ATH-SYO, and ATH-KAN-SYO) are shown on the top right corner of each panel. The location of noon (1200 MLT) is shown by black arrows. Figures 5a and 5c show that the shape of the simultaneous wave occurrence is a superposition of the wave occurrence at two stations shown in Figure 4. Namely, the KAN-SYO plot in Figure 5a shows higher occurrence when KAN and SYO are at morning-dayside sectors. The ATH-KAN plot in Figure 5c shows higher occurrence when ATH is in the morning sector and KAN is in the morning-dayside sectors. However, Figures 5b and 5d do not clearly show similar trends because of the smaller amount of data.

Table 2 shows the total available hours, total hours that waves are observed, and occurrence rates at one station and simultaneously at two or three stations. T_{KAN} and T_{sim} in the column of conditional probability in the line of KAN-SYO are the hour that waves are observed at KAN and the hour when waves are observed at both KAN and SYO simultaneously. Thus, the conditional probability in the right column of Table 2 is a proxy of the longitudinal extent of the waves, which is defined as the ratio of the number of hours that waves are simultaneously observed at two stations to the number of hours that waves are observed at one station.

Occurrence rates of ELF/VLF emissions at one station indicate that those at auroral latitudes (31% at KAN, 26% at SYO) are higher than those at subauroral latitudes(14% at ATH). The MLT differences between the KAN-SYO, ATH-SYO, and ATH-KAN pairs are 3, 8, and 11 h, respectively, and the simultaneous wave occurrence rates

Table 2. Wave Occurrence Rate and Spatial Extent

	Available (h)	Wave Hours (h)	Occurrence Rate (%)	Conditional Probability (%)
Athabasca	1042	144	14	
Kannuslehto	919	282	31	
Syowa station	271	71.5	26	
KAN-SYO	254	24.8	9.8	T_{sim}/T_{KAN} 36.8
(MLT 3 h difference)				T_{sim}/T_{SYO} 38.5
ATH-SYO	233	5.8	2.5	T_{sim}/T_{ATH} 31.5
(MLT 8 h difference)				T_{sim}/T_{SYO} 9.9
ATH-KAN	819	29.5	3.6	T_{sim}/T_{ATH} 30.4
(MLT 11 h difference)				T_{sim}/T_{KAN} 11.9
ATH-KAN-SYO	226	3.83	1.7	

decreased with these MLT differences by 9.8%, 2.5%, and 3.6%. The waves were simultaneously observed at all three stations for only 1.7% of time.

The conditional probability in Table 2 shows that at least 36.8% of the ELF/VLF emissions had a longitudinal extent of more than 3 h MLT. Because of the difference in wave occurrence at auroral and subauroral latitudes, about 30% of waves observed at subauroral latitudes are observed simultaneously with waves at auroral latitudes, whereas the opposite occurs for about 10% of waves at auroral latitudes.

3.3. Geomagnetic Activity

Table 3 shows the average *AE* and *Dst* indices for time intervals when waves are observed at only one station and when they are simultaneously observed at two or three stations (column labeled "Multiple") for the SYO-KAN, SYO-ATH, and KAN-ATH pairs, and SYO-KAN-ATH. The time intervals (wave hours) are also shown. Average *AE* and |*Dst*| are larger when the waves are simultaneously observed at more than two stations than when waves are observed at only one station throughout the entire data set. The average |*Dst*| index also tends to be larger with increasing MLT differences by −5.4 nT (SYO-KAN, 3 h), −15.3 nT (SYO-ATH, 8 h), and −28.8 nT (KAN-ATH, 11 h). On the other hand, the *AE* index does not depend clearly on the MLT differences, i.e., 70.7 nT (SYO-KAN, 3 h), 209 nT (SYO-ATH, 8 h), and 152 nT (KAN-ATH, 11 h). These two indices tend to be larger at subauroral latitudes (ATH), probably because large geomagnetic activity is necessary to inject high-energy plasma into the inner magnetosphere. For three stations where waves are simultaneously observed, the *AE* index is large (194 nT in SYO-KAN-ATH) but is close to the *AE* index for SYO-ATH, which is largest for the data set of two stations. The *Dst* index for SYO-KAN-ATH is nearly the mean value of the other two-station data sets.

Table 3. Average *AE*, *Dst* Indices and Wave Hours at Each Station or Multiple Stations for Each Data Set[a]

		Syowa Station	Kannuslehto	Athabasca	Multiple
SYO-KAN	$\overline{AE}(\sigma)$ (nT)	59.9 (71.6)	68.8 (79.6)		70.7 (111)
(MLT 3 h difference)	$\overline{Dst}(\sigma)$ (nT)	−3.2(14.9)	−4.0 (9.0)		−5.4 (15.8)
	Wave hours (h)	39.7	42.7		24.8
SYO-ATH	$\overline{AE}(\sigma)$ (nT)	51.5 (58.8)		126 (115)	209 (180)
(MLT 8 h difference)	$\overline{Dst}(\sigma)$ (nT)	−2.1 (15.1)		−4.7 (13.8)	−15.3 (16.9)
	Wave hours (h)	53.0		12.7	5.83
KAN-ATH	$\overline{AE}(\sigma)$ (nT)		101 (98.1)	145 (127)	152 (144)
(MLT 11 h difference)	$\overline{Dst}(\sigma)$ (nT)		−8.6 (13.1)	−9.1 (17.6)	−28.8 (25.9)
	Wave hours (h)		218	67.8	29.5
ATH-KAN-SYO	$\overline{AE}(\sigma)$ (nT)	58.3 (72.0)	68.1 (81.2)	146 (124)	194 (197)
	$\overline{Dst}(\sigma)$ (nT)	−2.6 (15.1)	−3.6 (12.0)	−6.7 (13.8)	−15.0 (19.8)
	Wave hours (h)	55.0	51.7	14.2	3.83

[a] σ, Standard deviation.

4. Discussion

We have estimated the occurrence rates of ELF/VLF emissions for 48 days at ATH, KAN, and SYO as a function of MLT. The occurrence rate of ELF/VLF emissions in Figure 4 is high at 0400–1100 MLT at ATH, at 0500–1900 MLT at KAN, and at 0300–1500 MLT at SYO. This result is basically consistent with those reported in previous literatures at auroral and subauroral latitudes. In both ground-based and satellite observations, chorus emission is predominantly observed in the morning sector at auroral latitudes [e.g., *Pope*, 1960; *Tsurutani and Smith*, 1977; *Spasojevic*, 2014] and at subauroral latitudes [e.g., *Martinez-Calderon et al.*, 2015b]. On the other hand, plasmaspheric hiss generally occurs between 1100 and 1900 MLT in the region $3 < L < 5$ [e.g., *Green et al.*, 2005; *Agapitov et al.*, 2011]. QP emissions is frequently observed in the dayside at auroral latitudes [e.g., *Sato et al.*, 1974; *Smith et al.*, 1998; *Engebretson et al.*, 2004; *Hayosh et al.*, 2014] and in the late morning to early afternoon at subauroral latitudes [e.g., *Martinez-Calderon et al.*, 2015b]. In the present analysis, the occurrence rate of chorus/hiss emissions is higher in the dayside sector at KAN and SYO in Figures 4b and 4c. This may be because the high flux of energetic electrons at the L value of KAN, even though some of them are lost to precipitate to the Earth in the morning sector during their drift to dayside. At further high latitudes at SYO ($L = 6.4$), the occurrence rates of ELF/VLF emissions drop again in the afternoon sector. This may be because the high-energy electron density is less at the L value at SYO than at KAN. The occurrence rate of chorus/hiss emissions and QP emissions at ATH is high between 0700 and 1200˜MLT (morning) in Figure 4a. This result is consistent with the previous study [*Martinez-Calderon et al.*, 2015b]. This may suggest that energetic electrons, which cause the temperature anisotropy, precipitate to the upper ionosphere along the magnetic field line before noon at subauroral latitudes (ATH, $L = 4.3$) and their density is insufficient to generate the ELF/VLF emissions in the afternoon.

The dayside preference of QP emission at KAN is also consistent with previous studies. These results may support the idea that one of the major causes of the QP emissions is the compressional ULF waves which mainly come from the dayside magnetosphere. However, no QP emission is observed at SYO in the present analysis, though *Sato et al.* [1974] made a statistical analysis of QP emissions using 2 years of the data from SYO. This may be due to a reduced number of wave events, smaller upper frequency limit (2.5 kHz), and less spectral quality at SYO. The data amount was not enough to statistically analyze the distribution of emissions as a function of wave type.

We also found that the fraction of QP emissions to all the ELF/VLF emissions at ATH at subauroral latitudes is higher than that at KAN near the auroral latitudes in Figure 4. On the other hand, *Engebretson et al.* [2004] showed that the QP emissions are observed more frequently in the auroral zone than at either higher or lower latitudes, based on multipoint ground measurements in Antarctica at magnetic latitudes from −62° (Halley) to −74° (South Pole). The ELF/VLF emissions generated at various L values are mixed to and become hiss emissions that have less temporal structures [e.g., *Bortnik et al.*, 2008, 2009; *Chen et al.*, 2009]. The low occurrence rate of QP emissions at auroral latitudes in the present study may be because the high occurrence of ELF/VLF emissions causes mixture of different waves to mask the QP emissions.

It is also known that electrons move from low to high L shells toward noon sector due to the effect of drift shell splitting [*Tsurutani and Smith*, 1977; *Li et al.*, 2009b; *Min et al.*, 2010]. This effect may also cause the low occurrence rate of emissions in the afternoon sector at subauroral latitudes. On the other hand, electrons moving from lower latitudes to higher latitudes due to drift shell splitting in anisotropic distributions may cause high occurrence rate of emissions at auroral L values in the afternoon sector.

We estimated simultaneous occurrence rates of ELF/VLF emissions statistically at two and three stations. Simultaneous wave occurrence rates are high when stations at auroral (subauroral) latitudes are in the dayside (morning) sector, namely SYO is at 0900–1200 MLT and KAN is at 1200–1500 MLT for the KAN-SYO pair, and ATH is at 0400–0900 MLT and KAN is at 1500–2000 MLT for the ATH-KAN pair (Figure 5). In other words, the simultaneous occurrence rates are higher when at least one station is in the morning sector and the other stations are in the dayside sector. This result may indicate that magnetospheric ELF/VLF emissions are not frequently observed in the premidnight sector because of the low density of energetic electrons for generating ELF/VLF emissions. On the contrary, the energetic electron density is higher from the postmidnight to morning sector due to the drift of the energetic electrons arising from the gradient and curvature of the ambient magnetic field. The temperature anisotropy of higher $T_\perp/T_\parallel$, which is essential to generate the ELF/VLF emissions, may occur in the dayside because of the precipitation of parallel electrons to the atmosphere in the morning sector [e.g., *Meredith et al.*, 2001; *Green et al.*, 2005].

As shown in Table 2, the simultaneous occurrence rate decreases with the MLT separation of the two stations. This may be partly because a large MLT separation increases the probability that one of the two stations is in the premidnight sector where the occurrence rate is very low. The conditional probability is greater than 9% in Table 2. This result indicates that at least 9% of ELF/VLF emissions are observed simultaneously on the global scale, possibly caused by the same triggers such as magnetic storms and substorms, and magnetospheric compressions.

Table 3 shows the average *AE* and *Dst* indices when waves are observed. The average *Dst* indices increase with increasing MLT differences. The average *AE* indices also increase with differences of more than 3 h MLT, although those do not clearly show dependence on differences of more than 8 h MLT. This result may indicate that simultaneous ELF/VLF emissions are mainly associated with high geomagnetic activity and that intense substorms must occur to observe the emissions at multiple stations simultaneously with larger MLT differences.

In this study, we assume that the extent of ELF/VLF emissions observed at multipoint ground stations represents the extent of generation region of the emissions in the magnetosphere. However, the effects of nonducted propagation should be also considered. By using a ray tracing simulation, *Chum and Santolik* [2005] demonstrated that nonducted propagation of waves toward lower L shells can occur depending on initial angles of waves in the generation region. *Golden et al.* [2010] reported that chorus waves observed on the ground at midlatitude stations propagate predominantly in the nonducted modes. Thus, nonducted propagation can affect the latitudinal extent of ELF/VLF emissions on the ground. However, longitudinal extent of ELF/VLF emissions may not be affected by nonducted propagation because wave duct is usually formed due to longitudinally nonuniform population of plasma density. In the future work, we need to investigate effects of longitudinal extension of waves during magnetosphere-ground propagation by using multipoint satellite observations and ray tracing modeling.

In our study, intensities of ELF/VLF emissions are different by more than 1 order of magnitude among three stations when waves are simultaneously observed (see, e.g., Figure 3). This difference is probably not only due to difference of wave intensities at the generation region but also due to attenuation during propagation through the ionosphere. *Ozaki et al.* [2009] have shown the effect of attenuation of ELF/VLF waves by the ionosphere based on the negative correlation between cosmic noise absorption and VLF intensities observed at West Ongul (near SYO) in Antarctica in the auroral zone.

Waves can be simultaneously observed at different stations with different intensities, frequencies, and structures, possibly due to attenuation of wave intensity during the propagation through the ionosphere, difference of cyclotron frequencies on different *L* values, and different background conditions, respectively. However, we could not estimate simultaneous wave occurrence rate as a function of wave types and frequencies, because of less number of data and different data sets of adequate quality at different stations. For QP emissions, simultaneous events at three stations were not found and data quality was not good enough to compare the modulation periods in detail even for simultaneous events at two stations. We would like to make such a detailed comparison of wave properties at multiple stations in future, if we obtain more continuous wave data set in better quality.

Although it is a rare case, we show a nearly simultaneous appearance of ELF/VLF hiss emissions at all three stations just after the passage of an enhancement of solar wind dynamic pressure in Figure 3. Similar appearance and enhancement of magnetospheric ELF/VLF emissions associated with sudden commencements/impulse events has been reported by *Hayashi et al.* [1968] and *Shiokawa et al.* [2014] on the ground-based stations. However, the present observation is the first multipoint observation of the enhancement of ELF/VLF emissions on the ground associated with the compression of the magnetosphere. The enhancement of solar wind dynamic pressure causes compression of the magnetosphere and subsequent betatron acceleration of high-energy magnetospheric electrons perpendicular to the magnetic field which results in the enhancement of temperature anisotropy to generate magnetospheric ELF/VLF emissions. The appearance was first at SYO at 1240 MLT (1235 UT), 1 min later at KAN at 1516 MLT, and 5 min later at ATH at 0440 MLT. This time difference may indicate propagation of the compression in the inner magnetosphere. If we assume an Alfven velocity of 1000 km/s, it takes 1 min to propagate 10 *Re*. Thus, the 5 min delay at ATH at 0440 MLT suggests that there is not only the time delay due to propagation speed of magnetospheric compression but also additional time delay (a few minutes) to generate the hiss emission in this morning sector. The response of generation

of ELF/VLF emissions to the magnetospheric compression will depend on the background condition of high-energy electrons and ambient plasma as well as magnetic field configuration.

5. Conclusion

We performed the first simultaneous ground-based observation of magnetospheric whistler mode wave emissions in the ELF/VLF range at stations in Canada and Finland, and Antarctica. We investigated the longitudinal extent of ELF/VLF emissions, including chorus/hiss and QP emissions. We also investigated their dependence on geomagnetic activity.

The occurrence rate of ELF/VLF emissions at subauroral latitudes (ATH) is high in the morning sector, whereas the ELF/VLF emissions at auroral latitudes (KAN and SYO) are mainly generated in the dayside sector. These results are consistent with previous studies at subauroral latitudes and auroral latitudes. The new findings in our study are summarized as follows.

1. The simultaneous occurrence rates at two stations are higher when the stations at auroral (subauroral) latitudes are in the dayside (morning) sector: SYO at 0900–1200 MLT and KAN at 1200–1500 MLT for the KAN-SYO pair; and ATH at 0400–0900 MLT and KAN at 1500–2000 MLT for the ATH-KAN pair. This may be because magnetospheric ELF/VLF emissions occur frequently in the morning sector at subauroral latitudes and in the dayside sector at auroral latitudes in relation to the distribution of density and temperature anisotropy of energetic electrons in the inner magnetosphere.
2. The simultaneous occurrence rate of ELF/VLF emissions decreases with the MLT separation of the two stations: 9.8% at KAN-SYO (ΔMLT=3 h), 2.5% at ATH-SYO (8 h), and 3.6% at ATH-KAN (11 h).
3. The probability of simultaneous wave observation when one station observed ELF/VLF emissions is at least 36% and 9% for the MLT differences of 3 and 8 h, respectively.
4. Average $|Dst|$ indices increase with increasing MLT differences when two stations observed ELF/VLF emissions simultaneously. The average *AE* indices are large with large MLT differences (8 and 11 h). This result suggests that simultaneous ELF/VLF emissions are associated with high geomagnetic activity.
5. We show the first multipoint observation of ELF/VLF hiss emissions associated with an enhancement of solar wind dynamic pressure. The ~5 min delay of hiss appearance at ATH at 0440 MLT from dayside (SYO at 1240 MLT) suggests that there is not only the propagation speed of magnetospheric compression but also additional time (a few minutes) to generate the hiss emission in this morning sector.
6. The fraction of QP emissions to all the ELF/VLF emissions is higher at subauroral latitudes (43% at ATH) than that at auroral latitudes (24% at KAN). This may be because the high occurrence of ELF/VLF emissions at auroral latitudes masks the QP emissions with a mixture of different waves.

These results show several interesting features on the longitudinal extent of magnetospheric ELF/VLF emissions on the ground. However, further study is required to understand the longitudinal extent of ELF/VLF emissions, including types of emissions and seasonal variation. More multipoint observations are needed to understand the spatial extent of ELF/VLF emissions statistically.

Acknowledgments
The ELF/VLF data at ATH are available from the Institute for Space-Earth Environmental Research (ISEE), Nagoya University. We express our gratitude to Y. Katoh, H. Hamaguchi, and Y. Yamamoto of ISEE for their continued technical support. Construction and operation of the Athabasca University Geophysical Observatory facilities is supported by the Canada Foundation for Innovation, and we thank Kyle Reiter for dedicated technical support. The OMNI data including solar wind parameters and geomagnetic indices used in this paper were obtained from the SPDF/GSFC OMNIWeb interface at http://omniweb.gsfc.nasa.gov/form/omni_min.html. The ELF/VLF wave data obtained at SYO, KAN, and ATH are available at the National Institute of Polar Research, Japan, Sodankyla Geophysical Observatory, University of Oulu, Finland, and ISEE, Nagoya University, Japan, respectively. This work was supported by the Inter-university Upper atmosphere Global Observation NETwork (IUGONET) of the Ministry of Education, Culture, Sports, Science and Technology (MEXT), Japan. We were also supported by the Grant-in-Aid for Scientific Research (20244080, 23403009, 25302006, 25247080, JP 15H05815, and JP 16H06286) from the Japan Society for the Promotion of Science.

References

Agapitov, O., V. Krasnoselskikh, Y. V. Khotyaintsev, and G. Rolland (2011), A statistical study of the propagation characteristics of whistler waves observed by Cluster, *Geophys. Res. Lett.*, *38*, L20103, doi:10.1029/2011GL049597.

Bortnik, J., R. M. Thorne, and N. P. Meredith (2008), The unexpected origin of plasmaspheric hiss from discrete chorus emissions, *Nature*, *452*, 62–66, doi:10.1038/nature06741.

Bortnik, J., W. Li, R. M. Thorne, V. Angelopoulos, C. Cully, J. Bonnell, O. Le Contel, and A. Roux (2009), An observation linking the origin of plasmaspheric hiss to discrete chorus emissions, *Science*, *324*, 775–778, doi:10.1126/science.1171273.

Bunch, N. L., M. Spasojevic, and Y. Y. Shprits (2012), Off-equatorial chorus occurrence and wave amplitude distributions as observed by the Polar Plasma Wave Instrument, *J. Geophys. Res.*, *117*, A04205, doi:10.1029/2011JA017228.

Chen, L., J. Bortnik, R. M. Thorne, R. B. Horne, and V. K. Jordanova (2009), Three-dimensional ray tracing of VLF waves in a magnetospheric environment containing a plasmaspheric plume, *Geophys. Res. Lett.*, *36*, L22101, doi:10.1029/2009GL040451.

Chen, L., J. Bortnik, W. Li, R. M. Thorne, and R. B. Horne (2012a), Modeling the properties of plasmaspheric hiss: 1. Dependence on chorus wave emission, *J. Geophys. Res.*, *117*, A05201, doi:10.1029/2011JA017201.

Chen, L., J. Bortnik, W. Li, R. M. Thorne, and R. B. Horne (2012b), Modeling the properties of plasmaspheric hiss: 2. Dependence on the plasma density distribution, *J. Geophys. Res.*, *117*, A05202, doi:10.1029/2011JA017202.

Chum, J., and O. Santolik (2005), Propagation of whistler-mode chorus to low altitudes: Divergent ray trajectories and ground accessibility, *Ann. Geophys.*, *23*(12), 3727–3738, doi:10.5194/angeo-23-3727-2005.

Carson, W. B., J. A. Koch, J. H. Pope, and R. M. Gallet (1965), Long-period very low frequency emission pulsations, *J. Geophys. Res.*, *70*(17), 4293–4303.

Dowden, R. L. (1971), Distinctions between mid latitude VLF hiss and discrete emissions, *Plant. Space Sci.*, *19*, 374–376.

Engebretson, M. J., J. L. Posch, A. J. Halford, G. A. Shelburne, A. J. Smith, M. Spasojevic, U. S. Inan, and R. L. Arnoldy (2004), Latitudinal and seasonal variations of quasiperiodic and periodic VLF emissions in the outer magnetosphere, *J. Geophys. Res.*, *109*, A05216, doi:10.1029/2003JA010335.

Golden, D. I., M. Spasojevic, F. R. Foust, N. G. Lehtinen, N. P. Meredith, and U. S. Inan (2010), Role of the plasmapause in dictating the ground accessibility of ELF/VLF chorus, *J. Geophys. Res.*, *115*, A11211, doi:10.1029/2010JA015955.

Golden, D. I., M. Spasojevic, W. Li, and Y. Nishimura (2012a), Statistical modeling of plasmaspheric hiss amplitude using solar wind measurements and geomagnetic indices, *Geophys. Res. Lett.*, *39*, L06103, doi:10.1029/2012GL051185.

Golden, D. I., M. Spasojevic, W. Li, and Y. Nishimura (2012b), An empirical modeling of magnetospheric chorus amplitude using solar wind and geomagnetic indices, *J. Geophys. Res.*, *117*, A12204, doi:10.1029/2012JA018210.

Green, J. L., S. Boardson, L. Garcia, W. W. L. Taylor, F. Fung, and B. W. Reinsch (2005), On the origin of whistler mode radiation in the plasmasphere, *J. Geophys. Res.*, *110*, A03201, doi:10.1029/2010JA016193.

Hayashi, K., S. Kokubun, and T. Oguti (1968), Polar chorus emission and worldwide geomagnetic variation, *Rep. Ionos. Space Res. Jpn.*, *22*, 149–160.

Hayosh, M., F. Němec, O. Santolik, and M. Parrot (2014), Statistical investigation of VLF quasiperiodic emissions measured by the DEMETER spacecraft, *J. Geophys. Res. Space Physics*, *119*, 8063–8072, doi:10.1002/2013JA019731.

Helliwell, R. A. (1965), *Whistler and Related Ionospheric Phenomena*, Stanford Univ. Press, Stanford, Cailf.

Horne, R. B., et al. (2005), Wave acceleration of electrons in the Van Allen radiation belts, *Nature*, *437*(7056), 227–230, doi:10.1038/nature03939.

Kennel, C. F., and H. E. Petschek (1966), Limit on stably trapped particle fluxes, *J. Geophys. Res.*, *71*(1), 1–28.

Kim, K.-C., Y. Shprits, J. Lee, and J. Hwang (2013), Empirically modeled global distribution of magnetospheric chorus amplitude using an artificial neural network, *J. Geophys. Res. Space Physics*, *118*, 6243–6253, doi:10.1002/jgra.50595.

Kim, K.-C., D.-Y. Lee, and Y. Shprits (2015), Dependence of plasmaspheric hiss on solar wind parameters and geomagnetic activity and modeling of its global distribution, *J. Geophys. Res. Space Physics*, *120*, 1153–1167, doi:10.1002/2014JA020687.

Li, W., R. M. Thorne, V. Angelopoulos, J. W. Bonnell, J. P. McFadden, C. W. Carlson, O. LeContel, A. Roux, K. H. Glassmeier, and H. U. Auster (2009a), Evaluation of whistler-mode chorus intensification on the nightside during an injection event observed in the THEMIS spacecraft, *J. Geophys. Res.*, *114*, A00C14, doi:10.1029/2008JA013554.

Li, W., R. M. Thorne, V. Angelopoulos, J. Bortnik, C. M. Cully, B Ni, O. LeContel, A. Roux, U. Auster, and W. Magnes (2009b), Global distribution of whistler-mode chorus wave observed on the THEMIS spacecraft, *Geophys. Res. Lett.*, *36*, L09104, doi:10.1029/2009GL037595.

Manninen, J. (2005), Some aspects of ELF-VLF emissions in geophysical research, PhD thesis, Univ. of Oulu, Oulu, Finland.

Manninen, J., N. G. Kleimenova, Y. V. Fedorenko, P. A. Bespalov, and T. Turunen (2014), New results of structured VLF emissions observed simultaneously at two closely located stations near $L \sim 5.5$, *Ann. Geophys.*, *32*, 1163–1167.

Manninen, J., T. Turunen, N. Kleimenova, M. Rycroft, L. Gromova, and I. Sirviö (2016), Unusually high frequency natural VLF radio emissions observed during daytime in Northern Finland, *Environ. Res. Lett.*, *11*, 124006, doi:10.1088/1748-9326/11/12/124006.

Martinez-Calderon, C., K. Shiokawa, Y. Miyoshi, M. Ozaki, I. Schofield, and M. Connors (2015a), Polarization analysis of ELF/VLF waves observed at subauroral latitudes during the VLF-CHAIN campaign, *Earth Planets Space*, *67*(1), 1–13, doi:10.1186/s40623-014-0178-7.

Martinez-Calderon, C., K. Shiokawa, Y. Miyoshi, M. Ozaki, I. Schofield, and M. Connors (2015b), Statistical study of ELF/VLF emissions at subauroral latitudes in Athabasca, Canada, *J. Geophys. Res. Space Physics*, *120*, 8455–8469, doi:10.1002/2015JA021347.

Meredith, N. P., R. B. Horne, and R. R. Anderson (2001), Substorm dependence of chorus amplitudes: Implications for the acceleration of electrons to relativistic energies, *J. Geophys. Res.*, *106*(A7), 13,165–13,178, doi:10.1029/2000JA900156.

Meredith, N. P., R. B. Horne, R. M. Thorne, and R. R. Anderson (2003), Favored regions for chorus-driven electron acceleration to relativistic energies in the Earth's outer radiation belt, *Geophys. Res. Lett.*, *30*(16), 1871, doi:10.1029/2003GL017698.

Meredith, N. P., R. B. Horne, R. M. Thorne, D. Summers, and R. R. Anderson (2004), Substorm dependence of plasmaspheric hiss, *J. Geophys. Res.*, *109*, A06209, doi:10.1029/2004JA010387.

Meredith, N. P., R. B. Horne, M. A. Clilverd, D. Horsfall, R. M. Thorne, and R. R. Anderson (2006), Origins of plasmaspheric hiss, *J. Geophys. Res.*, *111*, A09217, doi:10.1029/2006JA011707.

Min, K., J. Lee, and K. Keika (2010), Chorus wave generation near the dawnside magnetopause due to drift shell splitting of substorm-injected electrons, *J. Geophys. Res.*, *115*, A00I02, doi:10.1029/2010JA015474.

Miyoshi, Y., A. Morioka, T. Obara, H. Misawa, T. Nagai, and Y. Kasahara (2003), Rebuilding process of the outer radiation belt during the 3 November 1993 magnetic storm: NOAA and Exos-D observations, *J. Geophys. Res.*, *108*(A1), 1004, doi:10.1029/2001JA007542.

Miyoshi, Y., et al. (2015), Energetic electron precipitation associated with pulsating aurora: EISCAT and Van Allen Probe observations, *J. Geophys. Res. Space Physics*, *120*, 2754–2766, doi:10.1002/2014JA020690.

Omura, Y., M. Hikishima, Y. Katoh, D. Summers, and S. Yagitani (2009), Nonlinear mechanisms of lower-band and upper-band VLF chorus emissions in the magnetosphere, *J. Geophys. Res.*, *114*, A07217, doi:10.1029/2009JA014206.

Ozaki, M., S. Yagitani, I. Nagano, Y. Hata, H. Yamagishi, N. Sato, and A. Kadokura (2008), Localization of VLF ionospheric exit point by comparison of multipoint ground-based observation with full-wave analysis, *Polar Sci.*, *2*(4), 237–249.

Ozaki, M., S. Yagitani, I. Nagano, Y. H. Yamagishi, and N. Sato (2009), Estimation of enhanced electron density in the lower ionosphere using correlation between natural VLF emission intensity and CNA, *Nankyoku Shiryo (Antarctic Record)*, *53*(2), 123–135.

Parrot, M., and C. A. Gaye (1994), A statistical survey of ELF waves in a geostationary orbit, *Geophys. Res. Lett.*, *21*, 2463–2466, doi:10.1029/94GL01700.

Pope, J. (1960), Effect of latitude on the diurnal maximum of "dawn chorus", *Nature*, *185*, 87–88.

Sato, N., and S. Kokubun (1980), Interaction between ELF-VLF emissions and magnetic pulsations: Quasi-periodic ELF/VLF emissions associated with Pc 3-4 magnetic pulsations and their geomagnetic conjugacy, *J. Geophys. Res.*, *85*(A1), 101–113, doi:10.1029/JA085iA01p00101.

Sato, N., and H. Fukunishi (1981), Interaction between ELF/VLF emissions and magnetic pulsations: Classification of quasi-periodic ELF-VLF emissions based on frequency-time spectra, *J. Geophys. Res.*, *86*(A1), 19–29, doi:10.1029/JA086iA01p00019.

Sato, N., K. Hayashi, S. Kokubun, T. Oguti, and H. Fukunishi (1974), Relationships between quasi-periodic VLF emission and geomagnetic pulsation, *J. Atmos. Terr. Phys.*, *36*(9), 1515–1526.

Sazhin, S. S., and M. Hayakawa (1992), Magnetospheric chorus emissions: A review, *Planet. Space. Sci.*, *40*, 681–697, doi:10.1016/0032-0633(92)90009-D.

Shiokawa, K., et al. (2014), Ground-based ELF/VLF chorus observations at subauroral latitudes-VLF-CHAIN campaign, *J. Geophys. Res. Space Physics*, *119*, 7363–7379, doi:10.1002/2014JA020161.

Smith, A. J., M. J. Engebretson, E. M. Klatt, U. S. Inan, R. L. Arnoldy, and H. Fukunishi (1998), Periodic and quasiperiodic ELF/VLF emissions observed by an array of Antarctic stations, *J. Geophys. Res.*, *103*(A10), 23,611–23,622, doi:10.1029/98JA01955.

Smith, A. J., R. Horne, and N. Meredith (2010), The statistics of natural ELF/VLF waves derived from a long continuous set of ground-based observations at high latitude, *J. Atmos. Sol. Terr. Phys.*, *72*(5), 463–475.

Sonwalkar, V. S., and U. S. Inan (1989), Lightning as an embryonic source of VLF hiss, *J. Geophys. Res.*, *94*(A6), 6986–6994.

Spasojevic, M. (2014), Statistical analysis of ground-based chorus observations during geomagnetic storms, *J. Geophys. Res. Space Physics*, *119*, 8299–8317, doi:10.1002/2014JA019975.

Thorne, R. M., E. J. Smith, R. K. Burton, and R. E. Holzer (1973), Plasma-spheric hiss, *J. Geophys. Res.*, *78*, 1581–1596.

Tsurutani, B. T., and E. J. Smith (1977), Two types of magnetospheric ELF chorus and their substorm dependences, *J. Geophys. Res.*, *82*(32), 5112–5128, doi:10.1029/JA082i032p05112.